ELSEVIER

Journal of Quantitative Spectroscopy & Radiative Transfer 87 (2004) 53–67

Journal of Quantitative Spectroscopy & Radiative Transfer

www.elsevier.com/locate/jqsrt

Electromagnetic energy flow near nanoparticles—I: single spheres

Hongxing Xu*

Division of Solid State Physics, Lund University, Box 118, Lund 22100, Sweden

Received 10 June 2003; accepted 17 December 2003

Abstract

The electromagnetic (EM) energy flow near single spheres is investigated by applying Mie theory. From the patterns of the energy flow, the absorption and the scattering of light can be understood in the microscopic point of view. In the absorption profiles of metallic particles, most absorbed energy is consumed on the surface of the particles, which indicates that the resonance of surface plasmon is different from that of the bulk plasmon. Two mechanisms to enhanced local EM field are also distinguished. One is the surface plasmon resonance, and another one is the intensified energy flow.
© 2004 Elsevier Ltd. All rights reserved.

Keywords: Mie theory; Energy flow; Electromagnetic; Nanoparticles; Optical near field

1. Introduction

Although the fundamental understanding was performed almost a century ago by Mie, and probably Debye and Lorenz, the light scattering of small particles still obtains growing interests now due to the wide applications in various disciplines [1–3]. Recently, the fast development of nanooptics [4] and surface plasmon photonics [5] has allowed the detailed understanding of the light scattering of nanoparticles in nanometer scale. The interested near-field optical properties mainly include particle plasmons [3], enhanced local electromagnetic (EM) field [6,7], phase contrast of local EM field [8,9] and photonic force [10,11]. Together with the well-known far-field optical properties of extinction/scattering/absorption [2,3], the light scattering of small particles becomes a quite mature discipline.

In this paper, we will focus on another optical property of the EM energy flow near nanoparticles, which is a complementary of the above-mentioned optical properties. Such a study can be beneficial

* Fax: +46-46-222-3637.
E-mail address: hongxing.xu@ftf.lth.se (H. Xu).

0022-4073/$ - see front matter © 2004 Elsevier Ltd. All rights reserved.
doi:10.1016/j.jqsrt.2003.12.022

for further understanding of other optical properties. How the light is scattered/absorbed and how the local EM field is enhanced are naturally caused by the corresponding energy flow near nanoparticles. Moreover, the detailed optics and physics from this study can lead to useful applications as well, e.g. the heating of Au/Ag nanoparticles for catalysis to control the growth of nanowhiskers [12] and guiding light with small particles, which may be potentially applied in optical communication and sensor devices.

The basic assumption in this paper is the spherical shape of nanoparticles, from which the Mie theory [13] can be applied. The arrangement of this paper is as follows. In Section 2, we start out with the Mie theory. A modern form is presented in the appendix. In Section 3, we present the detailed energy flow in the inside/outside of metallic particles, and show how scattering/absorption spectra can be understood from the microscopic point of view. In Section 4, non-absorbed spheres are discussed. In Section 5, a summary is given.

2. The theory

In 1908, Gustav Mie developed the theory in order to understand how the different colors of small colloidal gold particles suspended in water vary with compositions [13]. Actually, this theory is the exact solution of EM scattering by a sphere of arbitrary radius and refractive index, embedded in an arbitrary homogeneous medium. Similar to all other EM problems, Mie theory is based on Maxwell's equations with appropriate boundary conditions. The mathematical trick was that Mie separated the spatial variables of the scalar EM potentials in spherical coordinates, i.e. $\psi = R(r)\Theta(\theta)\Phi(\phi)$, and solved the separate terms $R(r)$, $\Theta(\theta)$, $\Phi(\phi)$ independently. The scattered or penetrated EM fields are thus derived from the scalar EM potentials. Later on, Stratton [14] introduced a more formal mathematical approach, directly based on the partial components of the EM field: the transverse electrical field $\boldsymbol{M}_{\mathrm{mn}}$ and the transverse magnetic field $\boldsymbol{N}_{\mathrm{mn}}$ with $\boldsymbol{M} = \nabla \times (\boldsymbol{r}\psi)$, $\boldsymbol{N} = (1/k)\nabla \times \boldsymbol{M}$, $\boldsymbol{M} = (1/k)\nabla \times \boldsymbol{N}$. These partial fields have the form of vector spherical harmonics (VSHs). The partial components are divergence-free, i.e. $\nabla \bullet \boldsymbol{M} = 0$, $\nabla \bullet \boldsymbol{N} = 0$, and orthogonal, which are consistent with an EM field $(\boldsymbol{E}, \boldsymbol{H})$ in a homogeneous region. The scattering coefficients b_n and a_n, and the penetrated coefficients d_n and c_n can be deduced from the Maxwell boundary conditions. Thus, the analytical solution of the scattered field and penetrated field can be obtained [2,14]. The extinction/scattering/absorption cross sections can be then deduced for a plane-wave:

$$
\begin{aligned}
Q_{\mathrm{ext}} &= -\frac{2\pi}{k^2}\sum_{n=1}^{\infty}(2n+1)\mathrm{Re}(a_n + b_n),\\
Q_{\mathrm{s}} &= \frac{2\pi}{k^2}\sum_{n=1}^{\infty}(2n+1)(|a_n|^2 + |b_n|^2),\\
Q_{\mathrm{a}} &= Q_{\mathrm{ext}} - Q_{\mathrm{sca}}.
\end{aligned}
\tag{1}
$$

From the microscopic point-of-view, extinction, scattering and absorption relate to the total radiation affected by the particles, and can be calculated from integrals of energy flows for the different

types of electromagnetic fields that pass through an arbitrary surface A enclosing the particles. The energy flow is represented by the real part of the complex Poynting vector. Two types of energy flow: the total energy flow vector $\boldsymbol{S}$ and the scattered energy flow vector $\boldsymbol{S}_s$ are defined as

$$\boldsymbol{S} = \tfrac{1}{2}\,\mathrm{Re}(\boldsymbol{E} \times \boldsymbol{H}^*)$$

$$\boldsymbol{S}_s = \tfrac{1}{2}\,\mathrm{Re}(\boldsymbol{E}_s \times \boldsymbol{H}_s^*), \tag{2}$$

where the total electromagnetic field $[\boldsymbol{E}\ \boldsymbol{H}]$ is the sum of the incident field $[\boldsymbol{E}_i\ \boldsymbol{H}_i]$ and the scattered field $[\boldsymbol{E}_s\ \boldsymbol{H}_s]$ in the outside of the sphere, and the penetrated field $[\boldsymbol{E}_i\ \boldsymbol{H}_i]$ in the inside of the sphere, respectively.

Hence, the absorption/scattering/extinction cross-sections are originated from [14]:

$$Q_a = \frac{W_a}{S_0} = \frac{1}{S_0}\,\mathrm{Re}\int_A \boldsymbol{S} \bullet \boldsymbol{n}\,\mathrm{d}A,$$

$$Q_s = \frac{W_s}{S_0} = \frac{1}{S_0}\,\mathrm{Re}\int_A \boldsymbol{S}_s \bullet \boldsymbol{n}\,\mathrm{d}A,$$

$$Q_{ext} = -\frac{1}{2S_0}\,\mathrm{Re}\int_A [\boldsymbol{E}_i \times \boldsymbol{H}_s^* + \boldsymbol{E}_s \times \boldsymbol{H}_i^*] \bullet \boldsymbol{n}\,\mathrm{d}A, \tag{3}$$

where $\boldsymbol{n}$ is a unit vector pointing out from the closed surface A, and $S_0 = \frac{1}{2}\,\mathrm{Re}(\boldsymbol{E}_i \times \boldsymbol{H}_i)$ is the incident power. The absorption cross-section Q_a is the net energy flow into the surface A, which is dissipated in the particles if the surrounding medium is a non-absorbing material. Among Q_a, Q_s and Q_{ext}, only two cross-sections are independent, and needs to be calculated. Since the surface A in Eq. (3) is allowed to be arbitrary, it can be chosen to be any surface even enclosed only part of the particle. If so, the details of the absorption in each part of the particle can be calculated also.

More general, the EM energy flow, as a basic entity, can be calculated by Eq. (2), with no limit to the whole space if the EM field is known. Although it cannot convey more information than the classical EM field itself, it can show the more substantial physical picture that we are familiar with.

3. EM energy flow near metallic spheres

3.1. Au sphere

Fig. 1a shows the absorption spectrum of gold particle with the radius $r = 25$ nm calculated by Eq. (1), as an example to show how Mie theory successfully explains the red color of gold colloid. A strong absorption in the wavelength in the blue side of the absorption peak position of ~ 530 nm will absorb the blue light while allowing the red light to be transmitted. Let us investigate what happens in optical near field.

Fig. 1b–d shows the local EM energy flow (black lines) and the enhancement of the local electrical intensity (color) at the peak wavelength of 530 nm in three different planes (plane 1–3 illustrated in the inset of Fig. 1a). The enhancement of the local intensity out of the sphere is not homogenous. At the poles region aligned to the incident polarization, the intensity is enhanced about thirty times

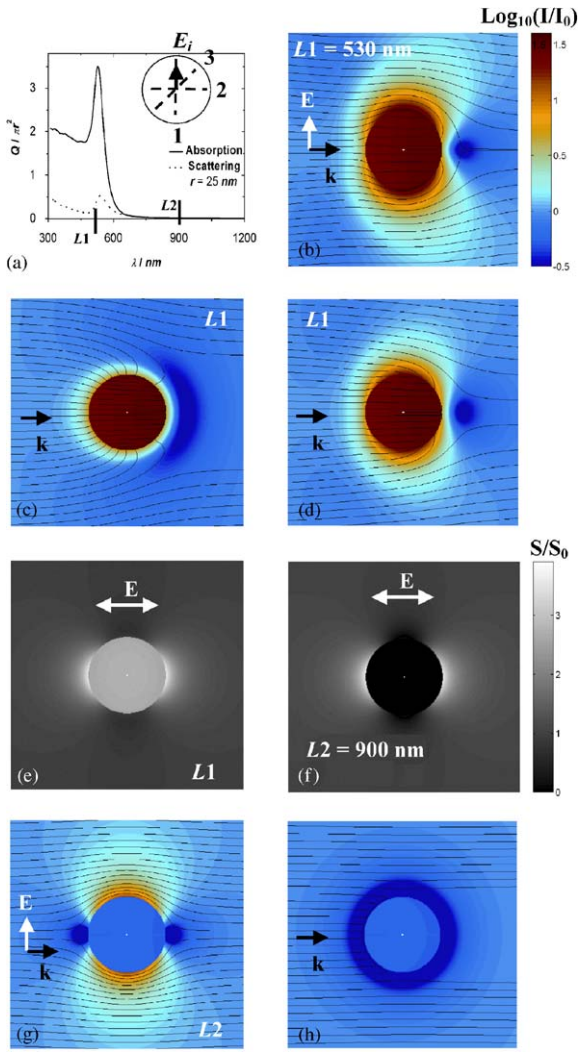

Fig. 1. (a) The absorption and scattering cross-sections of Au particle with the radius $r = 25$ nm in the water ($\varepsilon = 1.77$) vary with different incident wavelength λ; (b–d) and (g, h) the local electrical field enhancement in the logarithmic scale (color) and the energy flow (black lines) in the plane through the center of the sphere and parallel to the wave vector $\boldsymbol{k}$ illustrated in the inset of Fig. 1a, for (b) plane 1, (c) plane 2 and (d) plane 3 at the incident wavelength $L1 = 530$, and for (g) plane 1 and (h) plane 2 at $L2 = 900$ nm; (e, f) the density of the energy flow S/S_0 in the plane perpendicular to $\boldsymbol{k}$ and through the center of the sphere at the incident wavelength $L1 = 530$ nm for (e) and $L2 = 900$ nm for (f).

in Fig. 1b, while much less in the equator region as in Fig. 1c. Interestingly, the electric field in the inside of the particle is intensively enhanced. This indicates the strong excited surface plasmon modes that correspond to the strong penetrating electric field. But in Fig. 1g, at the longer wavelength, no enhancement in the inside of the Au particle can be observed, which indicates no excitations of surface plasmon modes. Nevertheless, it is clearly seen from the energy flow patterns that the “hot”

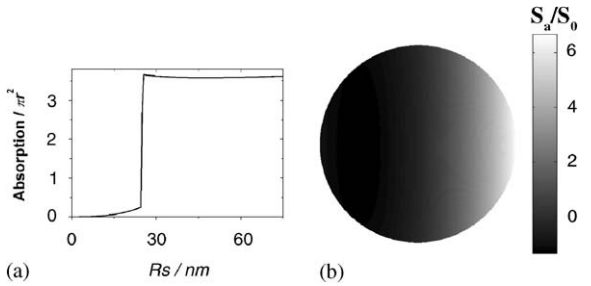

Fig. 2. (a) The absorption cross-sections in an enclosed spherical surface centered at the Au particle in Fig. 1 calculated by Eq. (3) vary with its radius Rs; (b) the density of the absorbed energy flow S_a/S_0 at the surface of the Au sphere with the incident wave vector $\boldsymbol{k}$ from the left to the right. The incident wavelength is $\lambda = 530$ nm. S_a is defined as $S_a = S_> - S_<$ when $Rs = r$, with $S_>$ for $Rs > r$ and $S_<$ for $Rs < r$.

particle in the blue side absorbed more light, while the "cold" particles in the red side corresponding to more transmission.

The patterns of the energy flow in the different planes are different, but there is no certain correlation to the enhancement of the local electrical field OUT the sphere. In the "hot pole" regions in Fig. 1b, where the electrical intensity is strongly enhanced, the density of the energy flow is not significantly denser compared to the incident energy flow far away from the particle. But in the same region in Fig. 1g, with a much longer incident wavelength of 900 nm, the density of energy flow is much denser, while the local electrical field is less enhanced as in Fig. 1b. For the former case, the enhanced local field is due to the excitations of surface plasmon modes, as a non-propagating wave, which stores EM energy for the excitations. But, the latter case at the non-resonance wavelength, the enhanced local field is contributed by the denser energy flow. Hence, we have two mechanisms to enhance the local field: one is the surface plasmon resonance (SPR), and another one is the intensified energy flow.

For the patterns of EM energy flow, we address three points here. Firstly, the energy flow is not homogenous surrounding the Au particle, even through the Au sphere itself is highly symmetric. The local energy flow strongly depends on the polarization and the incident wave vector. In Fig. 1b–d, the patterns of EM energy flow in the wave-front (left to the sphere) and at the back-side (to the right) are different due to the strong absorption of SPR. The difference between Fig. 1b and c is notable. The light is blocked more in Fig. 1c (plane 2, perpendicular to $\boldsymbol{E}_i$) than in Fig. 1b (plane 1 parallel to $\boldsymbol{E}_i$ and $\boldsymbol{k}$). This can be seen from the profile of the energy flow passing through the plane perpendicular to $\boldsymbol{k}$ and the center of the sphere in Fig. 1e. The reason for more light blocked in plane 2 is due to the antenna effect which transfers the EM energy flow to the oscillating electric current. This effect can be observed for the longer incident wavelength e.g. 900 nm as seen in Fig. 1f, h, although almost no absorption happens at this wavelength.

Secondly, most of the energy flow ends at the surface of the Au particle as seen in Fig. 1b–d, which means that the absorbed energy is mainly consumed at the surface of the Au particle. Fig. 2a shows the absorption in the inside of a closed spherical surface centered at the origin of the Au particle varies with the radius Rs calculated by Eq. (3). Only about 5% of the absorbed energy is consumed inside of the Au sphere, while 95% is consumed at the surface of the Au

sphere. The calculations for other sizes give a more or less similar result. Such a result would be quite surprising, but can be expected. From the EM theory [3], the resonant frequency of a surface plasmon mode for a metallic sphere roughly has the form of $\omega_l = \omega_p\sqrt{l/(2l+1)}$, where ω_p is the resonance frequency of the bulk metal. The dipole resonance thus occurs for $\omega = \omega_p/\sqrt{3}$, and higher orders happen at the even longer wavelengths. The resonant frequency for the surface modes is clearly different from the bulk resonance frequency. Hence, it is not stranger that much less energy is absorbed in the body comparing to the surface.

It is also worthwhile to address that the calculated absorption cross-section when $R_s > r$ by Eq. (3) is same as calculated by Eq. (1) with the value of $3.6\pi r^2$. When $R_s > r$, i.e. out of the sphere, there is no absorption source anymore. It would be easily expected that the calculated absorption should be a constant then. Fig. 2a shows it is the case by ignoring the small errors due to the surface integration. Messinger et al. [15] have defined a near-field form of the scattering cross-section Q_{NF}, which can be used to estimate the local field enhancement. They used the integration of E_{loc}^2 instead of the integration of the energy flow, i.e. the Poynting vector, as in Eq. (3). They found that Q_{NF} is strongly dependent on the distance to the particle. However, E_{loc}^2 is not necessarily equal to the energy flow in the optical near field as discussed above. One should not think that Q_a or Q_s will be different in the optical near field and the optical far field. Based on energy conservation, Q should be the same in the optical near field and the optical far field if the surrounding medium is the none-absorbed material.

Thirdly, the consuming of the absorbed EM energy is not homogenous at the surface, which can be seen from Fig. 2b. Most of the absorbed EM energy is consumed at the backside of the surface relative to the wave-front (to the right). Similar results are found for other sizes and other surrounding media as well. Due to the difference between the dielectric function of Au and water, the light track in the interface of water/Au in the wave-front and Au/water in the backside should be different. The dielectric function of Au is negative in the visible/infrared region, which is less than water $\varepsilon = 1.77$. More reflection will naturally happen when the light pass the interface from Au to water. This will increase the local EM energy intensity in the back surface. Thus more absorption can be expected.

For larger particles, the scattering become more significant due to the large size, while it can be ignored for small particle. As an example, Fig. 3a shows both the absorption and scattering of an Au sphere with the radius $r = 50$ nm. The maximum of the absorption is quite similar to that in Fig. 1a, but the absorption peak width becomes much broader. The scattering peak in Fig. 3a is almost twice than the absorption peak. Comparing to Fig. 1, the patterns of both the energy flow and the local field enhancement are different. The significant change is that the scattering can be observed from the patterns of energy flow. In Fig. 3c, the energy flow starts to disperse when it comes to the sphere from the left, which indicates the scattering effect. In Fig. 3f, where the incident wavelength is in the scattering peak position, the energy flow disperses even more. The profile of the scattering $\boldsymbol{S}_s$ on the surface of the particle can be visualized in Fig. 3d, where the scattering happens mainly in the area close to the equator, perpendicular to $\boldsymbol{E}_i$. Interestingly, the scattering photons by the part of the sphere facing the wave-front looks like the elastic collision of small particles by a sphere in Fig. 3d. The absorption effect can be seen from the convergence of the energy flow when it comes after the sphere in Fig. 3b, c, e and f. For the longer wavelength far away from that of SPR, there is no big difference between different sizes by comparing Figs. 3g,h to 1g,h.

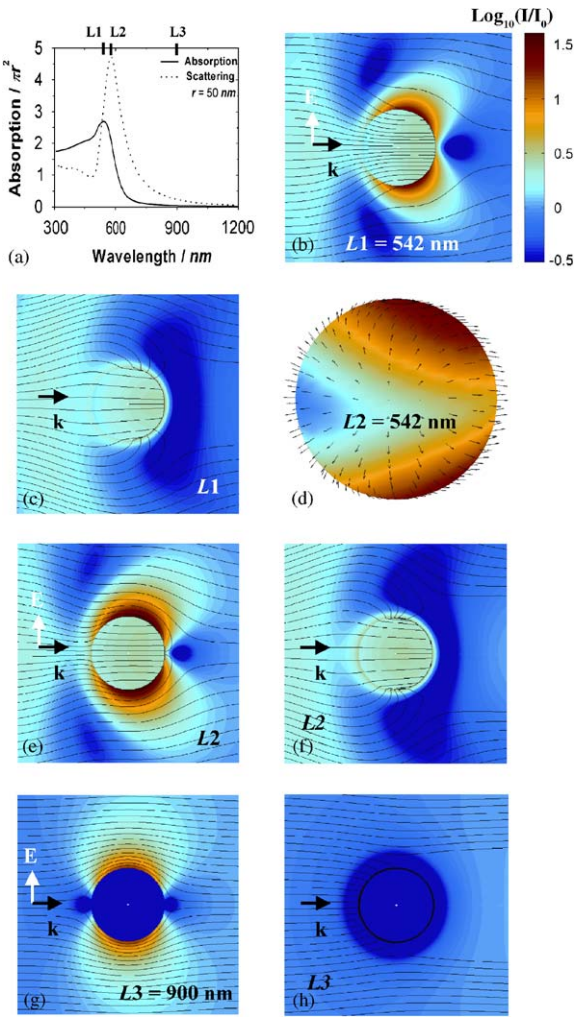

Fig. 3. (a) The absorption and scattering cross-sections of Au particle with the radius $r = 50$ nm in water vary with different incident wavelength λ; (b, c) and (e–h) the local electrical field enhancement in the logarithmic scale (color) and the energy flow (black lines) in plane 1 for (b) and plane 2 for (c) at the incident wavelength $L1 = 542$ nm, (e) for plane 1 and (f) plane 2 at $L2 = 577$ nm, and (g) for plane 1 and (h) plane 2 at $L3 = 900$ nm; (d) the scattering Poynting vector $\boldsymbol{S}_s$ calculated by Eq. (2) (arrows) and the local field distribution (color) at the surface of the Ag sphere.

3.2. Ag sphere

Recently, we have shown that silver particles have higher sensitivity of SPR influenced by the incident wavelength and the surrounding media than gold particles at the resonance condition due to a sharper disperse of the dielectric function of silver [16]. Here, we investigate how the sensitivity of SPR is relative to the absorption/scattering cross-section, the energy flow and the enhancement of the local field. The sharp SPR resonance peak for small particles e.g. $R = 10$ nm can be clearly seen in Fig. 4a, where the absorption is 17 times more than its geometric cross-section πr^2. This

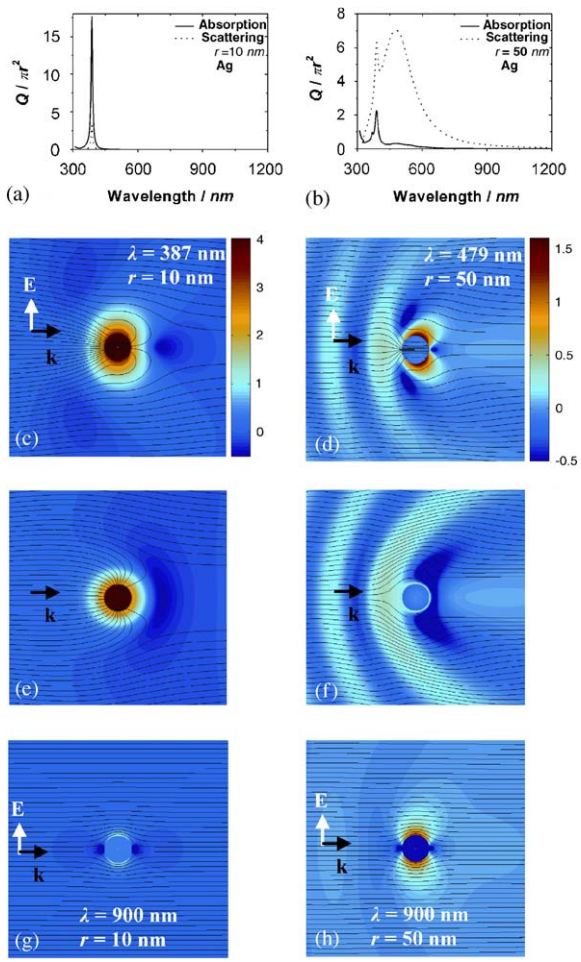

Fig. 4. The absorption and scattering cross-sections of Ag sphere with the radius $r = 10$ nm for (a) and $r = 50$ nm for (b) in water vary with different incident wavelength λ; and the local electrical field enhancement in the logarithmic scale (color) and the energy flow (black lines) in plane 1 for (c) and (e) plane 2 at the incident wavelength $\lambda = 387$ nm, and (g) plane 1 at the incident wavelength $\lambda = 900$ nm for $r = 10$ nm (colorbar to the left); and (d) for plane 1 and (f) plane 2 at the incident wavelength $\lambda = 479$ nm, and (h) plane 1 at the incident wavelength $\lambda = 900$ nm for $r = 50$ nm (colorbar to the right).

absorption cross-section is thirteen times more than that of the same size resonant Au sphere. In Fig. 4c and e, the shrink of the energy flow already starts far away from the Ag particle before the wave-front comes to it, which indicates the strong absorption. Hence, this near-field calculation is consistent with the calculated absorption cross-section in the far field.

The enhancement of the local intensity can be up to 10^4 in Fig. 4c, which is two orders more than that of Au particles. It is well-know that the enhancement of the local field is crucial for SERS. The enhancement factor of SERS roughly takes two power of the enhancement of the local field. Hence the enhancement factor of SERS can achieve about 10^8 in this case. Although this factor

is smaller than that of close-packed particles e.g. with the separation distance of about 1 nm as calculated in Ref. [7], it is quite close to the experimental enhancement factor required by single Hb molecule SERS [17]. Such a resonance is very sensitive to the incident wavelength. The particle is "hot" only when the incident wavelength is close to the resonant wavelength $\lambda = 387$ nm, while "cold" with more than 2 orders-of-magnitude lower enhancement immediately in other wavelength away from the absorption peak. Fig. 4g shows a "cold" particle for the incident wavelength $\lambda = 900$ nm.

For large Ag particles, the enhancement of the local field becomes weaker since the sharpness aligned to $\boldsymbol{E}_i$ will be decreased due to the larger radius. The scattering of large Ag particles becomes complex, which is similar to the case of large Au particles. The interference pattern of the local field between the incident light and the scattered light can be clearly seen in Fig. 4d and f in the left area to the sphere. The patterns of the energy flow also become more wave-like far away from the sphere.

For the different incident wavelength, the difference of the local field enhancement for large particle is mainly for the distribution of intensity as in Fig. 4d and f, while the important feature for the small particle is the difference in the absolute value of the intensity as in Fig. 4c and g. In Fig. 4d and f, the position of maximum intensity has moved from the right to the left with the increase of the incident wavelength, due of the in-phase requirement of the retarded scattered field and the incident field. For shorter wavelengths, the retardation effect becomes relatively stronger since the size of the particle becomes relative larger. Hence, one can find a more uneven local intensity distribution, and the position of the maximum intensity is shifted further to the right in Fig. 4d.

4. EM energy flow near non-absorbed spheres

For the non-absorbed spheres, the light scattering becomes relatively simple since no absorption need to be considered. Here we only consider two kinds of spheres: void spheres with the dielectric constant $\varepsilon = 1$ smaller than the surrounding medium e.g. water, and PMMA spheres with the dielectric function $\varepsilon = 2.22$ bigger than water. Fig. 5 shows the energy flow and the local field distribution near void spheres with different sizes, while Fig. 6 for the case of PMMA spheres. For the small size, both kinds of spheres do not influence much to the optical path as seen from the patterns of the energy flow. But the local intensity in the void is enhanced about 2 times as shown in Fig. 5a and b, while no significant enhancement for the PMMA sphere in Fig. 6a and b. When the size of the sphere is comparable to $\lambda/2$, the void disperses the light as seen in Fig. 5c and d, while the PMMA sphere focus the light as seen in Fig. 6c and d. The former case is due to the reflection in the interface of void/water, and the later case is similar as the principle of focus lenses. When the size of the sphere becomes even larger, both the patterns of the inference in the front of the sphere and the patterns of the diffraction in the back-side become significant as in Figs. 5g,h and 6g,h.

5. Summary

As a summary, we have presented the patterns of the energy flow surrounding spheres with different sizes and compositions. From these patterns, the light scattering and absorption can be well

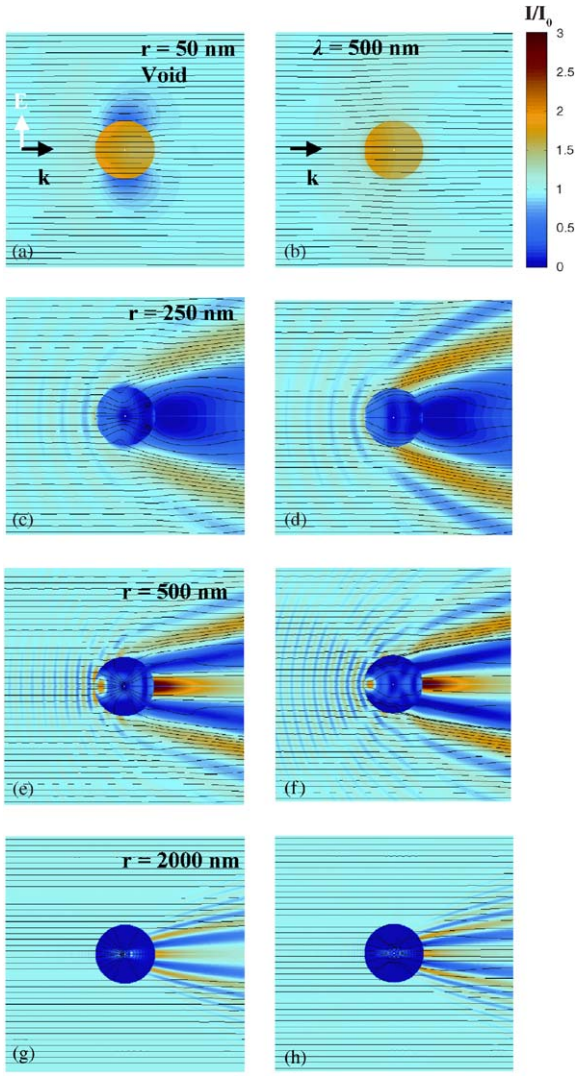

Fig. 5. The local electrical field enhancement in the linear scale (color) and the energy flow (black lines) surrounding a void sphere ($\varepsilon = 1$) in the water in plane 1 to the left and plane 2 to the right for (a,b) $r = 50$ nm; (c, d) $r = 250$ nm; (e, f) $r = 500$ nm; (g, h) $r = 2000$ nm at the incident wavelength $\lambda = 500$ nm.

understood in the nano-meter scale. The finding of the distribution of surface absorption for metallic particles could lead to the development of new heating methods for those particles, and possibly apply to study the temperature dependent catalysis. We also present two mechanisms to enhanced local electromagnetic field: the surface plasmon resonance and the intensified energy flow. Although the Mie theory for single particle is developed deeply in details, which could be possible simply as exercises in some text books, the studies for the optical details in the optical near field, e.g. the EM energy flow presented in this paper, can still lead some interesting results either in the research frontier or for the fundamental understanding.

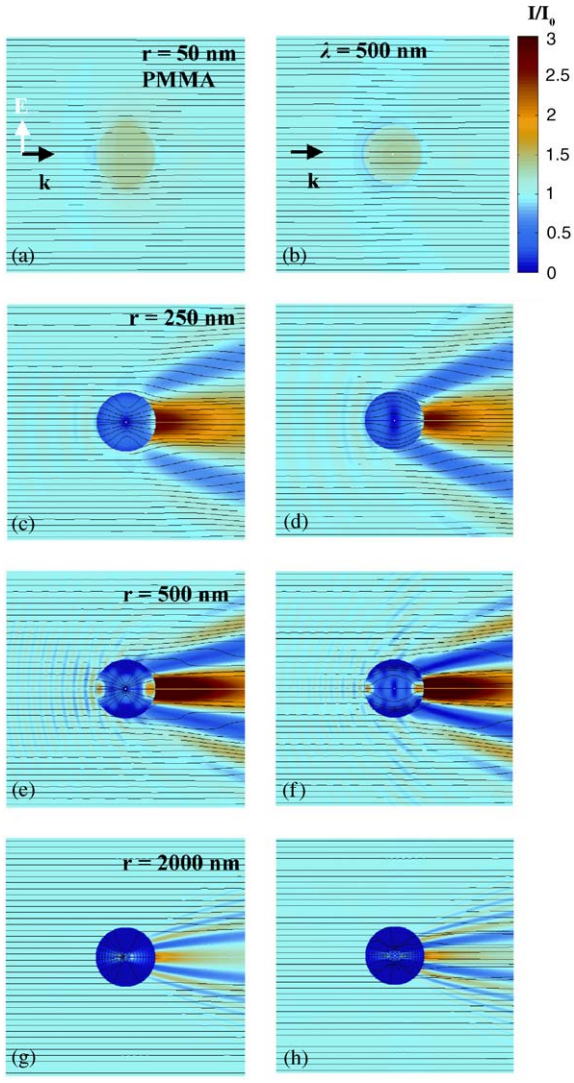

Fig. 6. Same as Fig. 5 but for a PMMA sphere ($\varepsilon = 2.22$).

Acknowledgements

The author gratefully acknowledges financial support from the Nanometer Consortium, Lund University, Sweden, the Swedish Foundation for Strategic Research and the Swedish Natural Science Research Council.

Appendix A. Expansion of a plane wave in VSHs

The critical issue in Mie theory is the expansion of the incident, scattered and penetrated EM fields in an infinite series of VSHs: M^j_{mn} and N^j_{mn}, which are defined in terms of spherical Bessel

functions $z_n^{(j)}$ [14] (corresponding to j_n, y_n, $h_n^{(1)}$, $h_n^{(2)}$ for $j=1,2,3,4$, respectively) and spherical harmonics Y_n^m as

$$M_{\mathrm{mn}} = (\hat{r},\hat{\theta},\hat{\phi}) \begin{bmatrix} 0 \\ \dfrac{1}{\sin\theta}\dfrac{\partial}{\partial\phi} \\ \dfrac{\partial}{\partial\theta} \end{bmatrix} z_n^{(j)}(kr) Y_n^m(\theta,\phi), \tag{A.1}$$

$$N_{\mathrm{mn}} = (\hat{r},\hat{\theta},\hat{\phi}) \begin{bmatrix} l(l+1) z_n^{(j)}(kr) \\ -\dfrac{\partial}{\partial r}\{z_n^{(j)} r(kr)\}\dfrac{\partial}{\partial\theta} \\ \dfrac{\partial}{\partial r}\{r z_n^{(j)}(kr)\}\dfrac{1}{\sin\theta}\dfrac{\partial}{\partial\phi} \end{bmatrix} \frac{1}{kr} Y_n^m(\theta,\phi),$$

where $\hat{r},\hat{\theta},\hat{\phi}$ are unit vectors; k is the absolute value of the wave vector $\boldsymbol{k}$; and $Y_n^m(\theta,\phi)$ is defined using associated Legendre functions P_n^m as $Y_n^m(\theta,\phi)=\sqrt{\frac{(2l+1)(n-m)!}{4\pi(n+m)!}} P_n^m(\cos\theta)\exp(\mathrm{i}m\varphi)$, and $P_n^m(x)=\frac{(1-x^2)^{m/2}}{2^l l!}\frac{d^{l+m}}{dx^{l+m}}(x^2-1)^l$ $h_n^{(1)}=j_n+\mathrm{i}y_n$, $h_n^{(2)}=j_n-\mathrm{i}y_n$. One should be aware that the spherical harmonics were not used in the original Mie theory, where $\exp(\mathrm{i}m\varphi)$ is written as a triangular function of either even or odd form [2,14]. However, the VSHs written here have a very concise form, which first appeared in the work of Inoue and Ohtaka [18] as the best of our knowledge. Additionally, since the spherical harmonics are generally used in quantum mechanics, many formula from quantum mechanics can be easily applied then as well, e.g. the calculation of Clebsch–Gorden coefficients for the vector coupling (coordinate translation) for the case of the ensemble of particles [19].

For convenient, the Dirac notations are borrowed (see [20]) to rewrite Eq. (A.1) as $|nmjp\rangle$ with $p=1$ for $\boldsymbol{M}$, and with $p=2$ for $\boldsymbol{N}$, respectively, where j represents different spherical Bessel functions. An incident plane wave $|i,E\rangle = \boldsymbol{E}_0 \mathrm{e}^{\mathrm{i}k\bullet r}$ can be expanded in an infinite series of VSHs as

$$|i,E\rangle = \sum_{n=1}^{\infty}\sum_{m=-n}^{n}\sum_{p=1}^{2} C_{\mathrm{mn}}^p \,|\, nm1\,p\rangle. \tag{A.2}$$

The expansion coefficients will have forms with $C_{\mathrm{mn}}^p = \langle nm1\,p|i\rangle / \langle nm1\,p|nm1\,p\rangle$ as

$$C_{\mathrm{mn}}^1 = \frac{2\pi i^n}{n(n+1)}\{-(iE_x-E_y)\sqrt{(n+m+1)(n-m)}\,Y_{n,m+1}^*(\hat{\boldsymbol{k}}) - (iE_x+E_y)\sqrt{(n-m+1)(n+m)}\,Y_{n,m-1}^*(\hat{\boldsymbol{k}}) + 2imE_z Y_{n,m}^*(\hat{\boldsymbol{k}})\}$$

$$C_{\mathrm{mn}}^2 = \frac{2\pi i^n}{n(n+1)}\left\{ n\sqrt{\frac{(n+m+1)(n+m+2)}{(2n+1)(2n+3)}}(iE_x-E_y)Y_{n+1,m+1}^*(\hat{\boldsymbol{k}}) - n\sqrt{\frac{(n-m+1)(n-m+2)}{(2n+1)(2n+3)}}(iE_x+E_y)Y_{n+1,m-1}^*(\hat{\boldsymbol{k}})\right.$$

$$-(n+1)\sqrt{\frac{(n-m-1)(n-m)}{(2n-1)(2n+1)}}(-iE_x+E_y)Y^*_{n-1,m+1}(\hat{k})$$

$$-(n+1)\sqrt{\frac{(n+m-1)(n+m)}{(2n-1)(2n+1)}}(iE_x+E_y)Y^*_{n-1,m-1}(\hat{\boldsymbol{k}})$$

$$+\left[2in\sqrt{\frac{(n+m+1)(n-m+1)}{(2n+1)(2n+3)}}\,Y^*_{n+1,m}(\hat{\boldsymbol{k}})-2i(n+1)\sqrt{\frac{(n+m)(n-m)}{(2n-1)(2n+1)}}\,Y^*_{n-1,m}(\hat{\boldsymbol{k}})\right]E_z\Bigg\},$$

The expansion of the magnetic field is easily obtained by applying the relations between the $\boldsymbol{E}$ field and the $\boldsymbol{H}$ field, and the relations between the normal modes

$$\boldsymbol{H}=\frac{1}{i\omega\mu}\nabla\times\boldsymbol{E},\quad \boldsymbol{N}=\frac{1}{k}\nabla\times\boldsymbol{M},\quad \boldsymbol{M}=\frac{1}{k}\nabla\times\boldsymbol{N}.$$

The magnetic field is thus expanded as

$$|i,H\rangle=\frac{1}{i\omega\mu}\sum_{n=1}^{\infty}\sum_{m=-n}^{n}\sum_{p\neq q=1}^{2}C^p_{\mathrm{mn}}\,|\,nm1q\rangle. \tag{A.3}$$

Appendix B. Scattering by a sphere

Each component of the transverse electrical and magnetic modes: $|nm11\rangle$ and $|nm12\rangle$, are diffracted with the scattering coefficients b_{mn} and a_{mn}, and the transmission coefficients d_{mn} and c_{mn}, respectively. At the same time, the normal modes for the scattered wave are changed to the spherical Hankel forms: $|nm31\rangle$ and $|nm32\rangle$ by simply changing the spherical Bessel functions j_n to $h^{(1)}_n=j_n+iy_n$ in Eq. (A.1). These changes are required by the multipole radiation field, i.e. the field must go to infinity at the origin of a multipole. Hence, the scattered and penetrated wave can be written as

$$|s,E\rangle=\sum_{n=1}^{\infty}\sum_{m=-n}^{n}C^1_{\mathrm{mn}}b_{\mathrm{mn}}|nm31\rangle+C^2_{\mathrm{mn}}a_{\mathrm{mn}}\,|\,nm32\rangle,$$

$$|s,H\rangle=\frac{k}{i\omega\mu}\sum_{n=1}^{\infty}\sum_{m=-n}^{n}(C^1_{\mathrm{mn}}b_{\mathrm{mn}}\,|\,nm32\rangle+C^2_{\mathrm{mn}}a_{\mathrm{mn}}\,|\,nm31\rangle),$$

$$|t,E\rangle=\sum_{n=1}^{\infty}\sum_{m=-n}^{n}C^1_{\mathrm{mn}}d_{\mathrm{mn}}|nm11\rangle+C^2_{\mathrm{mn}}c_{\mathrm{mn}}|nm12\rangle,$$

$$|t,H\rangle=\frac{k}{i\omega\mu}\sum_{n=1}^{\infty}\sum_{m=-n}^{n}(C^1_{\mathrm{mn}}d_{\mathrm{mn}}|nm12\rangle+C^2_{\mathrm{mn}}c_{\mathrm{mn}}|nm11\rangle). \tag{B.1}$$

The boundary conditions at the surface of the sphere satisfy Maxwell boundary conditions as

$$\begin{aligned}
&\boldsymbol{n}\times(\boldsymbol{E}_{\mathrm{i}}+\boldsymbol{E}_{\mathrm{s}})=\boldsymbol{n}\times\boldsymbol{E}_{\mathrm{t}}\\
&\boldsymbol{n}\times(\boldsymbol{H}_{\mathrm{i}}+\boldsymbol{H}_{\mathrm{s}})=\boldsymbol{n}\times\boldsymbol{H}_{\mathrm{t}},
\end{aligned}\tag{B.2}$$

where $\boldsymbol{n}$ is the unit normal vector pointing out from the surface and the subscript i, s and t represent the incident, scattered and penetrated wave, respectively. Each partial wave, with terms n and m, must fulfill these boundary conditions separately. Hence, Eq. (B.2) can be rewritten by plug in (B.1) as

$$\begin{aligned}
&\boldsymbol{n}\times(|nm11,kR\rangle+b_{\mathrm{mn}}|nm31,kR\rangle)=\boldsymbol{n}\times d_{\mathrm{mn}}|nm11,k_cR\rangle,\\
&\boldsymbol{n}\times\left(\frac{k}{i\omega\mu}|nm12,kR\rangle+\frac{k}{i\omega\mu}b_{\mathrm{mn}}|nm32,kR\rangle\right)=\boldsymbol{n}\times\frac{k_c}{i\omega\mu_c}d_{\mathrm{mn}}|nm12,k_cR\rangle,\\
&\boldsymbol{n}\times(|nm12,kR\rangle+a_{\mathrm{mn}}|nm32,kR\rangle)=\boldsymbol{n}\times c_{\mathrm{mn}}|nm12,k_cR\rangle,\\
&\boldsymbol{n}\times\left(\frac{k}{i\omega\mu}|nm11,kR\rangle+\frac{k}{i\omega\mu}a_{\mathrm{mn}}|nm31,kR\rangle\right)=\boldsymbol{n}\times\frac{k_c}{i\omega\mu_c}c_{\mathrm{mn}}|nm11,k_cR\rangle,
\end{aligned}\tag{B.3}$$

where R is the radius of the sphere, and k, k_c are the absolute values of the wave vector outside and inside the sphere, respectively. By combining Eqs. (A.1) and (B.3), we obtain the following four linear equations, which are equivalent to those found in [2,14]

$$\begin{aligned}
&j_n(kR)+b_{\mathrm{mn}}h_n^{(1)}(kR)=d_{\mathrm{mn}}j_n(k_cR),\\
&\frac{1}{\mu}[kRj_n(kR)]'+\frac{1}{\mu}b_{\mathrm{mn}}[kRh_n^{(1)}(kR)]'=\frac{1}{\mu_c}d_{\mathrm{mn}}[k_cRj_n(k_cR)]',\\
&\frac{1}{k}[kRj_n(kR)]'+\frac{1}{k}a_{\mathrm{mn}}[kRh_n^{(1)}(kR)]'=\frac{1}{k_c}c_{\mathrm{mn}}[k_cRj_n(k_cR)]',\\
&\frac{k}{\mu}j_n(kR)+\frac{k}{\mu}a_{\mathrm{mn}}h_n^{(1)}(kR)=\frac{k_c}{\mu_c}c_{\mathrm{mn}}j_n(k_cR).
\end{aligned}\tag{B.4}$$

In Eq. (B.4), we can easily find that the scattering and transmission coefficients a_{mn}, b_{mn}, c_{mn} and d_{mn} are independent of the angular term m, i.e. all m terms with the same n degenerate, and hence solved as:

$$\begin{aligned}
a_n&=-\frac{\mu_cj_n(\rho)[\eta j_n(\eta)]'-\mu\gamma^2j_n(\eta)[\rho j_n(\rho)]'}{\mu_ch_n^{(1)}(\rho)[\eta j_n(\eta)]'-\mu\gamma^2j_n(\eta)[\rho h_n^{(1)}(\rho)]'},\\
b_n&=-\frac{\mu_cj_n(\eta)[\rho j_n(\rho)]'-\mu j_n(\rho)[\eta j_n(\eta)]'}{\mu_cj_n(\eta)[\rho h_n^{(1)}(\rho)]'-\mu h_n^{(1)}(\rho)[\eta j_n(\eta)]'},\\
c_n&=\frac{\mu_ch_n^{(1)}(\rho)[\rho j_n(\rho)]'-\mu\gamma^2j_n(\rho)[\rho h_n^{(1)}(\rho)]'}{\mu_ch_n^{(1)}(\rho)[\eta j_n(\eta)]'-\mu\gamma^2j_n(\eta)[\rho h_n^{(1)}(\rho)]'},\\
d_n&=\frac{\mu_cj_n(\rho)[\rho h_n^{(1)}(\rho)]'-\mu h_n^{(1)}(\rho)[\rho j_n(\rho)]'}{\mu_cj_n(\eta)[\rho h_n^{(1)}(\rho)]'-\mu h_n^{(1)}(\rho)[\eta j_n(\eta)]'},
\end{aligned}\tag{B.5}$$

where $\gamma = k_c/k, \rho = kR$ and $\eta = k_c R$. The total electromagnetic field is simply the sum of the incident field and the scattered field as $|s+i,E\rangle$, $|s+i,H\rangle$ in the outside of the sphere, and $|t,E\rangle$, $|t,H\rangle$ in the inside of the sphere, respectively.

References

[1] Kerker M. The scattering of light and other electromagnetic radiation. New York: Academic press; 1969. p. 54–9.
[2] Bohren CF, Huffman DR. Absorbtion and scattering of light by small particles. New York: Wiley; 1983.
[3] Kreibig U, Vollmer M. Optical properties of metal clusters. New York: Springer; 1995.
[4] Ohtsu M. Near-field nano-optics. New York: Kluwer/Plenum; 2000.
[5] Euresco Conferences: Surface Plasmon Photonics, September 2003. p. 20–5.
[6] Moskovits M. Surface-enhanced spectroscopy. Rev Mod Phys 1985;57:783–826.
[7] Xu HX, Aizpurua J, Käll M, Apell P. Electromagnetic contributions to single-molecule sensitivity in surface-enhanced Raman scattering. Phys Rev E 2000;62:4318–24.
[8] Hillenbrand R, Keilmann F. Complex optical constants on a subwavelength scale. Phys Rev Lett 2000;85:3029–32.
[9] Prikulis J, Xu HX, Gunnarsson L, Käll M. Phase-sensitive near-field imaging of metal nanoparticles. J Appl Phys 2002;92:6211–3.
[10] Novotny L, Bian RX, Xie XS. Theory of nanometric optical tweezers. Phys Rev Lett 1997;79:645–8.
[11] Xu HX, Käll M. Surface-plasmon-enhanced optical forces in silver nanoaggregates. Phys Rev Lett 2002;89:246802.
[12] Björk MT, Ohlsson BJ, Sass T, Persson AI, Thelander C, Magnusson MH, Deppert K, Samuelson L, Wallenberg LR. One-dimensional heterostructures in semiconductor nanowhiskers. Appl Phys Lett 2002;80:1058–60.
[13] Mie G. Beitrage zur optik truber medien speziell kolloidaler metallösungen. Ann Phys 1908;25:377–445.
[14] Stratton JA. Electromagnetic theory. New York: McGraw-Hill; 1941.
[15] Messinger BJ, Vonraben KU, Chang RK, Barber PW. Local-fields at the surface of noble-metal microsphere. Phys Rev B 1981;24:649–57.
[16] Xu HX, Käll M. Modeling the optical response of nanoparticle-based surface plasmon resonance sensors. Sensor Actuat B 2002;87:244–9.
[17] Xu HX, Bjerneld EJ, Käll M, Börjesson L. Spectroscopy of single hemoglobin molecules by surface enhanced Raman scattering. Phys Rev Lett 1999;83:4357–60.
[18] Inoue M, Ohtaka K. Surface enhanced Raman-scattering by metal spheres .1. cluster effect. J Phys Soc Japan 1983;52:3853–64.
[19] Xu HX. A new method by extending Mie theory to calculate local field in outside/inside of aggregates of arbitrary spheres. Phys Lett A 2003;312:411–9.
[20] Sakurai JJ. Modern quantum mechanics. Reading, MA: Addison-Wesley; 1994. p. 10–4.